HHS Public Access

Author manuscript

J Phys Chem Lett. Author manuscript; available in PMC 2024 June 28.

Published in final edited form as:

J Phys Chem Lett. 2023 December 21; 14(50): 11480–11489. doi:10.1021/acs.jpclett.3c02444.

Substrate Positioning Dynamics Involves a Non-Electrostatic Component to Mediate Catalysis

Yaoyukun Jiang[1,#], **Ning Ding**[1,#], **Qianzhen Shao**[1,#], **Sebastian L. Stull**[1], **Zihao Cheng**[1], **Zhongyue J. Yang**[1,2,3,4,5,*]

[1]Department of Chemistry, Vanderbilt University, Nashville, Tennessee 37235, United States

[2]Center for Structural Biology, Vanderbilt University, Nashville, Tennessee 37235, United States

[3]Vanderbilt Institute of Chemical Biology, Vanderbilt University, Nashville, Tennessee 37235, United States

[4]Data Science Institute, Vanderbilt University, Nashville, Tennessee 37235, United States

[5]Department of Chemical and Biomolecular Engineering, Vanderbilt University, Nashville, Tennessee 37235, United States

Abstract

Substrate positioning dynamics (SPD) orients the substrate to reactive conformations in the active site, accelerating enzymatic reactions. However, it remains unknown whether SPD effects originate primarily from electrostatic perturbation inside the enzyme or can independently mediate catalysis with a significant non-electrostatic component. Here we investigated how the non-electrostatic component of SPD affects transition state stabilization. Using high-throughput enzyme modeling, we selected Kemp eliminase variants with similar electrostatics inside the enzyme but significantly different SPD. The kinetic parameters of these selected mutants were experimentally characterized. We observed a valley-shaped, two-segment linear correlation between the TS stabilization free energy (converted from kinetic parameters) and an index used to quantify SPD. Favorable SPD was observed for a distal mutant R154W, leading to the lowest activation free energy among the mutants tested. R154W involves an increased proportion of

[*]**Corresponding Author:** zhongyue.yang@vanderbilt.edu.

[#]Y. Jiang, N. Ding, and Q. Shao contributed equally.

Supporting Information. The following files are available free of charge. Detailed computational and experimental methods; folding free energy change upon mutation for 80 randomly generated single mutants of KE07-R7–2; constraints applied in the MD simulation; values of molecular dynamics-derived descriptors for the 15 variants; distribution of the snapshot electric field along the substrate breaking C–H bond for 14 KE07-R7–2 variants; primer sequences used in this study; Sanger sequencing chromatograms depicting site-directed mutagenesis in KE07-R7–2 variants; SDS-PAGE analysis of the purified KE07-R7–2 variants; scatter plots for the efficiency-enhancing free energy barrier changes upon mutation versus the substrate positioning index calculated using solvent-exclusive surface area; experimentally characterized kinetic parameters of the purified KE07-R7–2 variants; values of computed kinetic parameters for the 15 variants; decomposition of the change of transition state stabilization free energy upon mutation into k_{cat} and K_M components; correlation between the k_{cat} and K_M components of the effective activation free energy change upon mutation versus the substrate positioning index; solvent-accessible surface area decomposition of WT, N247W, and R154W mutants; the molecular mechanism underlying the impact of N247W and R154W mutations on enzyme kinetics; scatter plots for the correlation between the change of activation free energy versus the root-mean-square deviation from the idealized transition state. (PDF)
MD input files; workflow python script. (ZIP)

The authors declare no competing financial interest.

reactive conformations. These results indicate the contribution of the non-electrostatic component of SPD to mediating enzyme catalytic efficiency.

Graphical Abstract

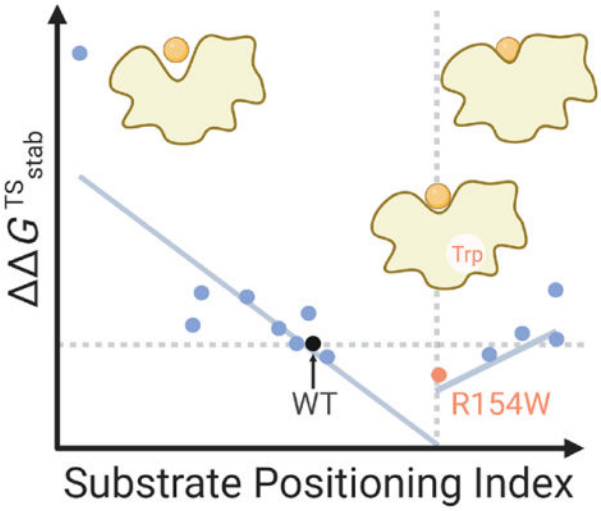

Keywords

Protein Dynamics; Enzyme Kinetics; Mutation Effect; Electrostatic Effect; Kemp Eliminase

Elucidating the catalytic origin of enzymes, a fundamental question in chemistry, guides the development of engineering strategies to create enzyme variants for chemical synthesis,[1–3] waste degradation,[4–7] fuel production,[8–11] disease diagnosis, and treatment.[12–14] Protein dynamics, which ranges over ten orders of magnitude,[15–24] have been widely reported to mediate catalysis.[17, 18, 25–28] For example, residue vibrations and collision have been proposed to facilitate transition state (TS) barrier crossing in the sub-picosecond time scale (e.g., lactate dehydrogenase, alcohol dehydrogenase, and purine nucleoside phosphorylase).[15–17] Residue and loop motions have been proposed to facilitate the positioning of substrates to form reactive conformation (or near-attack conformation[29]) in the pico- to nanosecond time scale (e.g., dihydrofolate reductase, chitinase, β-lactamase, retro-aldolase, Kemp eliminase, glycoside hydrolase, Cytochrome P450, and soybean lipoxygenase).[21–24, 30–37] Conformational change of loops and domains have been demonstrated to enable substrate binding, solvent shielding, or product releasing in the nanosecond to millisecond time scale (e.g., triosephosphate isomerase and adenylate kinase).[18, 19, 38, 39]

Substrate positioning dynamics (SPD) serves to orient the substrates for an energetically favorable barrier crossing and desired selectivity.[33, 36, 40–52] Experimentally, the impact of SPD on catalysis has been investigated using mutagenesis, where mutating dynamically-important residues results in a significant rate reduction (e.g., Gly121 in dihydrofolate reductase[53–56]). Furthermore, rate-enhancing mutants have been created through optimizing SPD.[49, 57] Broom *et al.* observed 700-fold rate acceleration in Kemp eliminase HG4

after multiple rounds of mutagenesis that turned out to rigidify the dynamic motion of active site residues.[49] However, a major pitfall of this mutagenesis-based approach is that SPD is coupled to the electrostatics inside enzyme,[25, 58] which is an established physical factor contributing to the high catalytic efficiency of enzymes based on theoretical,[59] computational,[34, 60–62] spectroscopy,[63–65] kinetic and mutagenesis studies.[58] Upon mutation, any change in SPD likely affects the projection of the enzyme electric field along the reacting bond. For instance, Wu *et al.* showed experimentally that the SPD mediates catalysis through tuning electrostatics in ketosteroid isomerase. This casts doubts on whether the correlation between the change of SPD and that of enzyme catalytic efficiency is confounded by electrostatics inside enzyme.[63]

We introduced eq. 1 and eq. 2 to quantitatively express the relationship between SPD and catalytic efficiency. Catalytic efficiency is represented by the transition state (TS) stabilization free energy,[66–70] denoted as $\Delta G^{\ddagger}_{stab}$, which stands for the difference in free energy between the enzyme-catalyzed transition state and the transition state in water (eq. 1 and Scheme 1). This quantity is first introduced by Wolfenden using a thermodynamic box to describe the catalytic origin of enzyme.[66, 68] The change of SPD affects $\Delta G^{\ddagger}_{stab}$ through two components: electrostatic stabilization energy $\Delta G_{ele}(SPD)$ and a non-electrostatic component $\Delta G_{nonele}(SPD)$ (eq. 2). To clarify, non-electrostatic component of SPD does not refer to non-electrostatic interactions between a substrate and enzyme residues but indicate the component of protein dynamics that mediates enzyme kinetics without perturbing interior electrostatics.

$$\Delta G^{\ddagger}_{stab} \equiv G^{TS,enzy} - G^{TS,water} \tag{1}$$

$$\Delta G^{\ddagger}_{stab}(SPD) = \Delta G_{ele}(SPD) + \Delta G_{nonele}(SPD) \tag{2}$$

Unless the impact of electrostatics is factored out in mutagenesis,[27, 71–73] it will remain unknown whether SPD originates primarily from electrostatic perturbation inside enzyme ($\Delta G_{nonele}(SPD) \approx 0$), or can independently mediate catalysis with a non-trivial $\Delta G_{nonele}(SPD)$. The answer to the question will not only deepen our fundamental understanding of the catalytic origin of enzymes but also inform whether dynamics-related descriptors should be considered as a general and independent factor for the computational engineering of biocatalysts. In this work, we investigated how the non-electrostatic component of SPD, $\Delta G_{nonele}(SPD)$, contributes to TS stabilization free energy, $\Delta G^{\ddagger}_{stab}$, using Kemp eliminase (KE07-R7–2) as a model enzyme.[35, 74] Through *in silico* high-throughput screening by EnzyHTP,[75] we identified single-point KE07-R7–2 mutants involving significantly different SPD but similar electrostatics inside enzyme ($\Delta G_{ele}(SPD) \approx 0$). We characterized the turnover rate and Michaelis constant of these mutants using biochemical assays. Based on these data, we investigated the correlation between the TS stabilization free energy and SPD to evaluate the contribution of $\Delta G_{nonele}(SPD)$.

Model System: Kemp Eliminase.

We used Kemp eliminase (KE),[34, 35, 39, 50, 61, 74, 76–79] the first *de novo*-designed enzyme, as the model enzyme in this study. The substrate 5-nitro-1,2-benzoxazole undergoes C–H deprotonation and ring opening catalyzed by a general base, generating 2-hydroxy-5-nitrobenzonitrile through a single transition state (Figure 1a *top*). In the KE07 series,[74] the general acid-base mechanism is enabled by active site residues, including Ala9, Ile11, Ser48, Trp50, Glu101, Tyr128, His201, Arg202, and Lys222 (Figure 1a *bottom*). Specifically, Glu101 serves as the general base that deprotonates the substrate, Lys222 acts as the hydrogen bond donor to stabilize the phenoxide intermediate, and Trp50 acts as the π-stacking residue to stabilize the substrate binding and charge-separated transition state. Four polar residues (Ser48, Tyr128, His201, and Arg202) stabilize the substrate binding or transition state through electrostatic or polar interactions. The nonpolar residues Ala9 and Ile11 likely favor substrate binding via dispersion interactions.

We employed KE07-R7–2, the KE variant out of seven rounds of directed evolution,[35, 74] as the wild-type (WT) scaffold. Three reasons support this choice. First, computational benchmarks[80] and biochemical assay protocols[81] have been established for KE07-R7–2, ensuring accuracy and reproducibility. Second, kinetic parameters have been experimentally characterized by Bhowmick *et al.*[35] for KE07-R7–2 mutants, providing references for this study. Third, both electrostatics inside the enzyme[61] and protein dynamics[35] are known to mediate catalytic efficiency of KE, making KE07-R7–2 a suitable model to investigate the electrostatic and non-electrostatic components of SPD.

Substrate Positioning Index.

To quantify the impact of protein dynamics on substrate positioning, we introduced a computational descriptor derived from molecular dynamics (MD) simulations. Existing descriptors for SPD, including mechanism-based bond parameters (e.g. length of a certain H-bond) and root-mean-square deviation (RMSD) of the active site, do not directly inform the dynamic response of substrate to the conformational fluctuation of the active site residues.[44, 49] Instead, we defined a substrate positioning index (SPI) based on solvent-accessible surface area (SASA, and see Figure S5 for the solvent-exclusive surface area test). SPI was determined by averaging the SASA ratio values calculated from individual snapshots extracted from the trajectories. Specifically, the SASA ratio between the substrate and active site residues (listed in Figure 1a *bottom*, selected based on previous benchmark[80]) was first computed for each snapshot, with $SASA_{sub}$ and $SASA_{pkt}$ calculated using isolated coordinates (as described in Text S1). Subsequently, these values were averaged across the conformational ensemble to derive the SPI value (i.e., $\langle SASA_{sub}/SASA_{pkt} \rangle$, Figure 1b).

When the same substrate binds to different enzyme mutants, a higher SPI value indicates that protein dynamics leads to a tighter positioning of the substrate in the active site. As such, SPI quantitatively describes SPD:

$$SPD = SPD(SPI) \tag{3}$$

This descriptor was first introduced in our prior study of mutation effects in lactonase *Sso*Pox,[46] where a piecewise linear correlation was observed between the activation free energies and SPI values for various lactonase mutant-substrate pairs. An optimal range of SPI was identified that enables the non-native substrate to react as efficiently as the native substrate.

KE Mutant Selection.

We designed a high-throughput computational workflow to identify single amino acid mutations with significant variation in SPD (represented by SPI, eq. 3) but minimal change in electrostatics inside enzyme (Figure 2), therefore approximating $\Delta G_{ele}(SPD)$ to zero (eq. 2). Electrostatics inside enzyme is represented by the electric field (EF) change of the breaking C–H bond relative to the WT, ΔEF_{C-H} (Text S1). Using EnzyHTP,[75, 82] we constructed the high-throughput computational workflow to build structural models for 98 KE variants, identify thermally stable mutants using a folding stability test at room temperature (Table S1), and eventually perform a functional test to select mutations that perturb SPI significantly but electric field minimally (Figure 2a and Table S2).

The 98 KE variants used in this study consist of 1 wild-type enzyme (KE07-R7–2[39, 74]), 17 mutants reported by Bhowmick *et al.*[35] and involved in our previous benchmark study,[80] and 80 randomly-generated mutants using EnzyHTP.[75] The 80 randomly generated mutants were first tested for folding stability using Rosetta *cartesian_ddg*[83, 84] to minimize unexpressed and misfolded mutants. Through the stability test, 61 mutants were retained with their folding free energies of less than 10 Rosetta Energy Units. These mutants were used for the following MD simulations, in which the average SPI and ΔEF_{C-H} were calculated using snapshots sampled from MD production trajectories. Structural constraints were applied throughout the MD simulations to enhance the sampling of enzyme conformations that stabilize pre-reaction complexes (Figure S1). To calculate $\Delta EFC2010033_H$, we first calculated the electric field strength projected along the breaking C–H bond of the substrate (EF_{C-H}) in each MD snapshot. The EF_{C-H} was summed at the middle point of the C–H bond from all partial charges of protein atoms. Then the relative electric field change, ΔEF_{C-H}, was calculated as the difference between the average EF_{C-H} of a mutant and the WT: $\Delta EF_{C-H} = \langle EF_{C-H}^{mutant} \rangle - \langle EF_{C-H}^{WT} \rangle$.

To factor out the impact of electrostatics, we selected the mutants whose averaged electric field strength was determined to be within ±2.88 MV/cm compared to the wild-type enzyme (KE07-R7–2). This range corresponds to the fluctuation of electrostatic stabilization energy (ΔG_{ele}) of ±0.1 kcal/mol, in which ΔG_{ele} was estimated by the projection of the electric field on the reacting dipole of C–H bond (Text S1). Within these variants, we further selected 5 KE variants for a kinetic assessment, including N247W, K4M, R154W, K37Q, and WT. These variants are evenly distributed across an SPI range from 1.30 to 1.70 (orange dots in Figure 2c) with an interval between 0.12 and 0.15.

After the first round of kinetic measurements, R154W was found to exhibit a 1.4-fold increase in k_{cat}/K_M compared to the WT (Tables S4 and S5). We further selected D14F (from our random mutants) and E185A (characterized by Bhowmick *et al.*[35]) for the

second round of kinetic measurement (white dots in Figure 2c) because they contribute additional data points for mutants that possess an SPI value greater than that of R154W. These mutation sites are distant from the active site and from each other (Figure 2b). In addition to these 7 mutants, we identified another 7 mutants from the study of Bhowmick *et al.*,[35] including H201A, M62A, N25S, K162A, K132M, H84Y, and L170A. Their projected electric field strengths also fall within ±2.88 MV/cm compared to KE07-R7–2. We thus obtained 14 variants for experimental characterization. Despite nearly identical averaged electric field strengths in the 14 mutants compared to the WT, a potential factor affecting the results may stem from multiple conformations, causing multimodal distribution of electric field strength. To test this possibility, we calculated the distributions of electric field strength for the 14 variants. Only single-peak $EF_{C–H}$ distribution is observed for all variants (Figure S2). This means that conformational diversity is unlikely to affect the results.

We measured the kinetic parameters for the 14 selected variants, and converted their turnover number k_{cat} and Michaelis constant K_M values to the change of TS stabilization free energy upon mutation[85] (i.e.,$\Delta\Delta G^{TS}_{stab}$) using eq. 4:

$$\Delta\Delta G^{TS}_{stab} \approx \Delta\Delta G^{\ddagger}_{eff} = -RT\ln\frac{k^{mutant}_{cat}/K^{mutant}_{M}}{k^{WT}_{cat}/K^{WT}_{M}} \quad (4)$$

In this equation, K_M approximates to be dissociation constant, k_{cat}/K_m approximates the apparent rate constant, and thus $\Delta\Delta G^{\ddagger}_{eff}$ approximates the change of the apparent activation free energy upon mutation. According to Scheme 1, $\Delta\Delta G^{\ddagger}_{eff}$ approximates to the change of ΔG^{TS}_{stab} upon mutation (i.e.,$\Delta\Delta G^{TS}_{stab}$). Temperature T is set at 298 K and R represents the gas constant. Since $\Delta G_{nonele}(SPD) \approx 0$, combining eq. 2–4 leads to:

$$\Delta\Delta G^{TS}_{stab}(SPI) = \Delta\Delta G_{ele}(SPI) + \Delta\Delta G_{nonele}(SPI) \approx \Delta\Delta G_{nonele}(SPI) \quad (5)$$

This relation allows us to investigate the contribution of non-electrostatic component of substrate-positioning dynamics ($\Delta\Delta G_{nonele}$) directly from the change of TS stabilization free energy $(\Delta\Delta G^{TS}_{stab})$. Upon change of SPI, a trivial change in $\Delta\Delta G^{TS}_{stab}(SPI)$ indicates that SPD originates primarily from electrostatic perturbation inside enzyme, while a significant change in $\Delta\Delta G^{TS}_{stab}(SPI)$ indicates that SPD independent mediates catalysis with a substantial non-electrostatic component.

Non-electrostatic Component of Substrate Positioning Dynamics.

Based on eq. 5, we performed correlation analysis between $\Delta\Delta G^{TS}_{stab}$ and SPI to evaluate non-electrostatic component of SPD. A valley-shaped, two-segment piecewise linear correlation was observed between $\Delta\Delta G^{TS}_{stab}$ and SPI values for the 14 selected KE variants (Figure 3a). The first linear segment involves a gradual drop of $\Delta\Delta G^{TS}_{stab}$ from 1.7 kcal/mol (H201A) to −0.2 kcal/mol (R154W), which accompanies the increase of SPI value from 1.17 (H201A) to 1.56 (R154W). The second linear segment involves a gradual increase of $\Delta\Delta G^{TS}_{stab}$ from −0.2

kcal/mol (R154W) to 0.3 kcal/mol (K37Q), which accompanies the increase of SPI value from 1.56 (R154W) to 1.68 (K37Q). The Pearson correlation coefficients for the two linear segments are −0.83 and 0.83, respectively. R154W exhibits the most favorable $\Delta\Delta G^{TS}_{stab}$ value with an SPI of 1.56. The observed outcomes demonstrate a strong statistical significance, as the error bars of $\Delta\Delta G^{TS}_{stab}$ values show minimal overlap among the seven variants chosen from our computational mutagenesis (e.g., N247W, WT, K4M, R154W, D14F, E185A, and K37Q). The largest standard error is only 0.05 kcal/mol for N247W, which is half of the electrostatic stabilization energy selection window (i.e., 0.1 kcal/mol). Despite H201A appearing as an outlier, the removal of this data point does not disrupt the linear correlation on the left linear segment, which maintains a Pearson correlation coefficient of −0.82.

The correlation shown in Figure 3a indicates the non-trivial contribution of non-electrostatic component of SPD in catalysis, with $\Delta\Delta G_{nonele}$ changing from −0.2 to 1.7 kcal/mol upon variation of SPI. Although $\Delta\Delta G^{TS}_{stab}$ has been observed to change 3–7 kcal/mol upon variation of electric field inside enzyme through mutagenesis,[64] an unfavorable SPD can substantially disrupt catalysis. As an example, we experimentally characterized the kinetic parameters for S48N (gray dot in Figure 3a). This mutant involves a favorable electrostatic environment (a $\Delta EF_{C–H}$ of 5.68 MV/cm), but a small SPI value (1.23) that substantially deviates from the predicted optimal range (1.56). The $\Delta\Delta G^{TS}_{stab}$ value of S48N was measured to be +1.56 kcal/mol, which is >10-fold slower than the wild-type enzyme at room temperature. This negative impact of substrate-positioning dynamics is projected to be even worse if the favorable electrostatic contribution is factored out in S48N.

According to eq. 4, $\Delta\Delta G^{TS}_{stab}$ can be decomposed to contributions from k_{cat} $\left(\Delta\Delta G^{\ddagger}_{k_{cat}} = -RT\ln\frac{k_{cat}^{mutant}}{k_{cat}^{WT}}\right)$ and $K_M\left(\Delta\Delta G^{\ddagger}_{K_M} = -RT\ln\frac{K_M^{mutant}}{K_M^{WT}}\right)$. To identify the key factor influencing the valley-shaped curve, we separately examined the correlation of SPI with $\Delta\Delta G^{\ddagger}_{k_{cat}}$ and $\Delta\Delta G^{\ddagger}_{K_M}$ (Text S2 and Figure S6). The result shows that $\Delta\Delta G^{\ddagger}_{k_{cat}}$ dominates the valley-shaped trend except for the outlier N247W, while $\Delta\Delta G^{\ddagger}_{K_M}$ exhibits minimal dependence on SPI. Notably, in our previous work for lactonase *Sso*Pox, we observed a similar trend between $\Delta\Delta G^{\ddagger}_{k_{cat}}$ and SPI.[46] A recent study by Bååth *et al.*[86] showed that the turnover of poly(ethylene terephthalate) hydrolases also follows a valley-shaped trend,[87, 88] where the turnover rate is initially enhanced and then diminished as the monotonic decrease of enzyme-substrate binding affinity (Sabatier principle).

Substrate Positioning Dynamics Mediates the Sampling of Reactive Conformations.

The increase of SPI from 1.17 to 1.68 reflects the process in which mutations reshape protein dynamics, gradually positioning the substrate toward a more compact active-site conformation. As such, we hypothesized that the non-electrostatic component of SPD mediates enzyme kinetics by perturbing the population of reactive conformation. To validate this hypothesis, we calculated the mass-weighted RMSD relative to the active site of the idealized transition state (iTS),[74] i.e., $RMSD_{iTS}$, for each KE variant, and tested their correlation to SPI. $RMSD_{iTS}$ was calculated by considering all heavy substrate atoms, as

well as C_α and side chains of Trp50, Glu101, and Lys222 amino acid residues, using the Röthlisberger et al. model as the reference structure[74]. The structural model of iTS is shown in Figure 3b. Using this structure as the reference, we calculated the mass-weighted RMSD of each MD snapshot as $\mathrm{RMSD}_{\mathrm{iTS}} = \sqrt{\frac{\sum_{i=1}^{N} m_i (X_i - X_{\mathrm{iTS}})^2}{M}}$, where X represents the coordinate of an atom, i denotes the i^{th} atom in this snapshot, and iTS denotes the corresponding atom in the reference iTS structure. m_i is the mass of the i^{th} atom. N is the total number of heavy atoms and M is the total mass. We have confirmed that $\mathrm{RMSD}_{\mathrm{iTS}}$ is an effective descriptor for reactive conformation population with a decent linear correlation (Pearson coefficient = 0.82, Figure S8).

As shown in Figure 3c, the correlation between the average $\mathrm{RMSD}_{\mathrm{iTS}}$ and SPI values also follows a valley-shaped, two-segment piecewise linear trend. The $\mathrm{RMSD}_{\mathrm{iTS}}$ decreases from 1.14 Å (H201A) to 0.88 Å (K132M) as SPI increases from 1.17 (H201A) to 1.56 (R154W) whereas $\mathrm{RMSD}_{\mathrm{iTS}}$ starts to increase beyond the SPI value of 1.56 and reaches a local maximum of 1.03 Å in D14F. The Pearson coefficients for the two fitting lines are −0.87 and 0.36. This result informs more physical details behind the valley-shaped correlation pattern. During the first linear segment, the increase of SPI leads to the reduction of active-site pocket space, which enhances the sampling of reactive conformations that resemble the active-site geometry of an idealized TS. However, when the pocket further shrinks and surpasses the optimal SPI range, the active site tends to populate in a non-reactive conformation that deviates significantly from the iTS. As such, the non-electrostatic component of SPD promotes enzyme kinetics by shifting the conformation ensemble towards TS-like geometries. This may help lower the conformational entropy cost during the transition from reactant to transition state. This two-segment piecewise linear correlation trend may exist universally in enzymes when electrostatic contributions are factored out, which is similar to the “volcano plot” or Sabatier principle broadly observed in catalysis[89]. The specific SPI value for optimal enzyme kinetics, however, is likely to be case-dependent.

To understand the molecular mechanism of how mutations mediate substrate positioning dynamics, we conducted conformational analyses on R154W (SPI = 1.56) and compared it against the results of WT (SPI = 1.42). As shown in Figure 4a, R154W is a remote mutation located on the surface of the enzyme and is spatially distant from the active site (i.e., ~19.4 Å away from the active site). Compared to the WT, the $\mathrm{SASA}_{\mathrm{pkt}}$ of R154W decreases by 18.30 Å^2. To identify which residue contributes the most to the change of active-site pocket, we decomposed the $\mathrm{SASA}_{\mathrm{pkt}}$ into contributions of individual residues (Table S6). The decomposition shows that Trp50 contributes over 84% of the overall decrease. As shown in Figure 4b, the large reduction in $\mathrm{SASA}_{\mathrm{pkt}}$ is driven by the shortening of spatial proximity between Trp50 and Ser144. This is supported by the downshift of distance distribution between Ser144 O_γ and Trp50 H_ε $\left(d_{O_\gamma - H_\varepsilon}\right)$ upon mutation (average $d_{O_\gamma - H_\varepsilon}$ values: 4.45 Å in R154W; 6.87 Å in WT, Figure 4c *left*). Furthermore, the formation of hydrogen bond between Ser144 O_γ and Trp50 H_ε is observed in R154W (around 2.72 Å) but is absent in WT.

Compared to WT, the close contact between Ser144 and Trp50 eliminates the accessible space of the substrate, forcing it to adopt a conformation that is parallel to the sidechain of

Trp50 (Figure 4b). This conformation directs the breaking C–H bond towards the carboxylic group of Glu101. The $RMSD_{iTS}$ distribution of R154W shifts towards smaller values, generating more conformations that resemble the iTS (Figure 4c *right*). This likely reduces the activation entropy cost, which ultimately reduces the activation barrier. Notably, a similar phenomenon has been observed in HG3, another member of the Kemp eliminase family.[57] Otten *et al.* showed that the evolved HG3 variants have more ordered side-chain orientations, leading to optimal positioning of the residues crucial to the chemical transformation and constraining of the ligand in the reactive pose.

In summary, we combined computational and experimental approaches to investigate the non-electrostatic component of substrate positioning dynamics (SPD) in mediating enzyme kinetics using Kemp eliminase (KE) as a model system. To quantitatively describe SPD, we introduced a molecular dynamic-derived descriptor, substrate positioning index (SPI), which is defined using the ratio of solvent-accessible surface area between the substrate and the enzyme active site residues. We designed a high-throughput computational workflow to identify stable KE variants that involve similar electrostatics inside enzyme but distinct SPI values.

The resulting KE variants were characterized using kinetic assays. The correlation between activation free energies and SPI values demonstrates a valley-shaped, two-segment piecewise linear relationship. The trend was validated using additional KE data reported by Bhowmick *et al.*[35] The presence of an optimal SPI value was observed in R154W, which corresponds to the lowest activation free energy among the selected mutants. We further investigated the relationship between SPI and the root-mean-square deviation of each conformational ensemble from an idealized active-site transition state model. The results show that the non-electrostatic component of SPD promotes enzyme kinetics by shifting the conformation ensemble towards TS-like geometries. To understand the molecular details behind how mutation reshapes the SPD, we performed conformational analyses on R154W and compared the results against the WT. We found that this distal mutation has a significant impact on the conformational distribution at the active site, where the mutation enables a hydrogen bonding between Ser144 and Trp50, limiting the accessible space of the substrate and positioning the substrate towards chemical activation.

These results indicate the presence of a non-electrostatic component of SPD in mediating enzyme catalysis. To promote catalysis, SPD has to position the substrate in an optimal active-site cavity to favor barrier crossing. The study implies that SPD should be considered as an independent factor in developing strategies for pinpointing rate-enhancing mutants for biocatalysis. The study also highlights SPI as a descriptor that informs the impact of the mutation on substrate positioning dynamics. SPI can be easily calculated from molecular mechanical modeling and implemented in high-throughput computational workflows for computational enzyme engineering. On a separate note, statistical energy (E_{MaxEnt}), which quantifies the fitness of a specific sequence in evolution, has been recently demonstrated to display a strong anti-correlation[90] (correlation values are −0.88 and −0.89 for $\log(k_{cat}/K_M)$ and $\log k_{cat}$, respectively) to the corresponding activity ($\log(k_{cat}/K_M)$ or $\log k_{cat}$) in the KE variants reported by Bhowmick *et al.*[35] Although E_{MaxEnt} is different from SPI, further investigations into the relationship between substrate positioning dynamics and the

evolutionary profile of sequences may inform the synergy between the free energy landscape and fitness landscape that mediates enzyme catalysis in evolution.[57]

Computational and Experimental Methods

Computational Methods.

We employed EnzyHTP, a software developed by our lab, to perform high-throughput computational screening of Kemp eliminase (KE) mutants.[75] A job script was prepared that leveraged EnzyHTP functions to automate the process of enzyme structure preparation, random mutation generation,[91] folding stability assessment,[83, 84] molecular dynamics simulation using AMBER18,[91] quantum mechanics calculation using Gaussian16[92] and TeraChem,[93, 94] and post-analysis of results using PyMol.[95] The workflow starts from KE07-R7–2,[39] the "wild-type" structure used in this study and then creates and simulates 98 random KE variants with single amino acid substitution. The configurations of the EnzyHTP functions are detailed in Text S1.

Experimental Methods and Characterization.

The enzymes were expressed in *Escherichia coli* BL21(DE3) using a pET-29b(+) vector (Novagen) and purified using Ni-NTA resin (Invitrogen). Kinetic parameters were determined using 5-nitro-1,2-benzoxazole as the substrate, with concentrations ranging from 5 to 1500 μM. The reactions were initiated by adding 50 μL of the enzyme (8 μM final concentration) to 150 μL of the substrate in a 96-well plate (Corning-Costa) at 25 °C in 25 mM HEPES (pH 7.25), 100 mM NaCl, 5% glycerol and 1.5% (v/v) acetonitrile.[35] The formation of the product was monitored at 380 nm using a SpectraMax iD3 microplate reader (Molecular Device). V_{max} and K_m were calculated by nonlinear regression with the Michaelis-Menten model using GraphPad Prism software (Version 8).[96] Three biologically independent replicates were used to calculate means and standard deviations. More details can be found in Text S1.

Supplementary Material

Refer to Web version on PubMed Central for supplementary material.

ACKNOWLEDGMENT

This research was supported by the startup grant from Vanderbilt University. Z. J. Yang, Y. Jiang, N. Ding, and Q. Shao are supported by the National Institute of General Medical Sciences of the National Institutes of Health under award number R35GM146982. Z. J. Yang thanks the sponsorship from Rosetta Commons Seed Grant Award and the Dean's Faculty Fellowship in the College of Arts and Science at Vanderbilt. S. L. Stull acknowledges financial support from the 24 Vanderbilt Undergraduate Summer Research Program and the Department of Computer Science. This work used SDSC Dell Cluster with AMD Rome HDR IB at Expanse from the Advanced Cyberinfrastructure Coordination Ecosystem: Services & Support (ACCESS) program, which is supported by National Science Foundation grants BIO200057.[97]

REFERENCES

(1). Koeller KM; Wong C-H Enzymes for Chemical Synthesis. Nature 2001, 409, 232–240, DOI: 10.1038/35051706. [PubMed: 11196651]

(2). Strohmeier GA; Pichler H; May O; Gruber-Khadjawi M Application of Designed Enzymes in Organic Synthesis. Chem. Rev 2011, 111, 4141–4164, DOI: 10.1021/cr100386u From NLM Medline. [PubMed: 21553913]

(3). Petchey MR; Grogan G Enzyme-Catalysed Synthesis of Secondary and Tertiary Amides. Adv. Synth. Catal 2019, 361, 3895–3914, DOI: 10.1002/adsc.201900694.

(4). Austin HP; Allen MD; Donohoe BS; Rorrer NA; Kearns FL; Silveira RL; Pollard BC; Dominick G; Duman R; El Omari K; et al. Characterization and Engineering of a Plastic-Degrading Aromatic Polyesterase. Proc. Natl. Acad. Sci. U. S. A 2018, 115, E4350–E4357, DOI: 10.1073/pnas.1718804115. [PubMed: 29666242]

(5). Knott BC; Erickson E; Allen MD; Gado JE; Graham R; Kearns FL; Pardo I; Topuzlu E; Anderson JJ; Austin HP; et al. Characterization and Engineering of a Two-Enzyme System for Plastics Depolymerization. Proc. Natl. Acad. Sci. U. S. A 2020, 117, 25476–25485, DOI: 10.1073/pnas.2006753117 From NLM Medline. [PubMed: 32989159]

(6). Tiso T; Narancic T; Wei R; Pollet E; Beagan N; Schroder K; Honak A; Jiang M; Kenny ST; Wierckx N; et al. Towards Bio-Upcycling of Polyethylene Terephthalate. Metab. Eng 2021, 66, 167–178, DOI: 10.1016/j.ymben.2021.03.011 From NLM Medline. [PubMed: 33865980]

(7). Ellis LD; Rorrer NA; Sullivan KP; Otto M; McGeehan JE; Román-Leshkov Y; Wierckx N; Beckham GT Chemical and Biological Catalysis for Plastics Recycling and Upcycling. Nat. Catal 2021, 4, 539–556, DOI: 10.1038/s41929-02100648-4.

(8). Chundawat SP; Beckham GT; Himmel ME; Dale BE Deconstruction of Lignocellulosic Biomass to Fuels and Chemicals. Annu. Rev. Chem. Biomol. Eng 2011, 2, 121–145, DOI: 10.1146/annurev-chembioeng-061010-114205. [PubMed: 22432613]

(9). Yang B; Dai Z; Ding S-Y; Wyman CE Enzymatic Hydrolysis of Cellulosic Biomass. Biofuels 2011, 2, 421–449, DOI: 10.4155/bfs.11.116.

(10). Sweeney MD; Xu F Biomass Converting Enzymes as Industrial Biocatalysts for Fuels and Chemicals: Recent Developments. Catalysts 2012, 2, 244–263.

(11). Horn SJ; Vaaje-Kolstad G; Westereng B; Eijsink VG Novel Enzymes for the Degradation of Cellulose. Biotechnol. Biofuels 2012, 5, 45, DOI: 10.1186/1754-6834-545 From NLM PubMed-not-MEDLINE. [PubMed: 22747961]

(12). Gordon SR; Stanley EJ; Wolf S; Toland A; Wu SJ; Hadidi D; Mills JH; Baker D; Pultz IS; Siegel JB Computational Design of an Alpha-Gliadin Peptidase. J. Am. Chem. Soc 2012, 134, 20513–20520, DOI: 10.1021/ja3094795. [PubMed: 23153249]

(13). Sun S; Jiang D; Fan M; Li H; Jin C; Liu W Selection of a Versatile Lactobacillus Plantarum for Wine Production and Identification and Preliminary Characterisation of a Novel Histamine-Degrading Enzyme. Int. J. Food Sci. Technol 2020, 55, 2608–2618, DOI: 10.1111/ijfs.14514.

(14). Samadi N; Heiden D; Klems M; Salzmann M; Rohrhofer J; Weidmann E; Koidl L; Jensen-Jarolim E; Untersmayr E Gastric Enzyme Supplementation Inhibits Food Allergy in a BALB/c Mouse Model. Nutrients 2021, 13, DOI: 10.3390/nu13030738 From NLM Medline.

(15). Saen-oon S; Quaytman-Machleder S; Schramm VL; Schwartz SD Atomic Detail of Chemical Transformation at the Transition State of an Enzymatic Reaction. Proc. Natl. Acad. Sci. U. S. A 2008, 105, 16543–16548, DOI: 10.1073/pnas.0808413105. [PubMed: 18946041]

(16). Schwartz SD; Schramm VL Enzymatic Transition States and Dynamic Motion in Barrier Crossing. Nat. Chem. Biol 2009, 5, 552–559, DOI: 10.1038/nchembio.202.

(17). Schwartz SD Protein Dynamics and Enzymatic Catalysis. J. Phys. Chem. B 2023, DOI: 10.1021/acs.jpcb.3c00477.

(18). Henzler-Wildman KA; Lei M; Thai V; Kerns SJ; Karplus M; Kern D A Hierarchy of Timescales in Protein Dynamics Is Linked to Enzyme Catalysis. Nature 2007, 450, 913–U927, DOI: 10.1038/nature06407. [PubMed: 18026087]

(19). Henzler-Wildman KA; Thai V; Lei M; Ott M; Wolf-Watz M; Fenn T; Pozharski E; Wilson MA; Petsko GA; Karplus M; et al. Intrinsic Motions Along an Enzymatic Reaction Trajectory. Nature 2007, 450, 838–U813, DOI: 10.1038/nature06410. [PubMed: 18026086]

(20). Hanson JA; Duderstadt K; Watkins LP; Bhattacharyya S; Brokaw J; Chu JW; Yang H Illuminating the Mechanistic Roles of Enzyme Conformational Dynamics. Proc. Natl. Acad. Sci. U. S. A 2007, 104, 18055–18060, DOI: 10.1073/pnas.0708600104. [PubMed: 17989222]

(21). Bhabha G; Lee J; Ekiert DC; Gam J; Wilson IA; Dyson HJ; Benkovic SJ; Wright PE A Dynamic Knockout Reveals That Conformational Fluctuations Influence the Chemical Step of Enzyme Catalysis. Science 2011, 332, 234–238, DOI: 10.1126/science.1198542. [PubMed: 21474759]

(22). Agarwal PK; Billeter SR; Rajagopalan PTR; Benkovic SJ; Hammes-Schiffer S Network of Coupled Promoting Motions in Enzyme Catalysis. Proc. Natl. Acad. Sci. U. S. A 2002, 99, 2794–2799, DOI: 10.1073/pnas.052005999. [PubMed: 11867722]

(23). Cannon WR; Singleton SF; Benkovic SJ A Perspective on Biological Catalysis. Nat. Struct. Biol 1996, 3, 821–833, DOI: 10.1038/nsb1096-821. [PubMed: 8836096]

(24). Epstein DM; Benkovic SJ; Wright PE Dynamics of the Dihydrofolate-Reductase Folate Complex - Catalytic Sites and Regions Known to Undergo Conformational Change Exhibit Diverse Dynamical Features. Biochemistry 1995, 34, 11037–11048, DOI: 10.1021/bi00035a009. [PubMed: 7669761]

(25). Welborn VV Structural Dynamics and Computational Design of Synthetic Enzymes. Chem. Catalysis 2022, 2, 19–28, DOI: 10.1016/j.checat.2021.10.009.

(26). Petrovic D; Kamerlin SCL Molecular Modeling of Conformational Dynamics and Its Role in Enzyme Evolution. Curr. Opin. Struct. Biol 2018, 52, 50–57, DOI: 10.1016/j.sbi.2018.08.004. [PubMed: 30205262]

(27). Kamerlin SCL; Warshel A At the Dawn of the 21st Century: Is Dynamics the Missing Link for Understanding Enzyme Catalysis? Proteins 2010, 78, 1339–1375, DOI: 10.1002/prot.22654. [PubMed: 20099310]

(28). Radkiewicz JL; Brooks CL Protein Dynamics in Enzymatic Catalysis: Exploration of Dihydrofolate Reductase. J. Am. Chem. Soc 2000, 122, 225–231, DOI: 10.1021/ja9913838.

(29). Hur S; Bruice TC The near Attack Conformation Approach to the Study of the Chorismate to Prephenate Reaction. Proc. Natl. Acad. Sci. U. S. A 2003, 100, 12015–12020, DOI: 10.1073/pnas.1534873100. [PubMed: 14523243]

(30). Watney JB; Agarwal PK; Hammes-Schiffer S Effect of Mutation on Enzyme Motion in Dihydrofolate Reductase. J. Am. Chem. Soc 2003, 125, 3745–3750, DOI: 10.1021/ja028487u. [PubMed: 12656604]

(31). Hammes-Schiffer S Impact of Enzyme Motion on Activity. Biochemistry 2002, 41, 13335–13343, DOI: 10.1021/bi0267137. [PubMed: 12416977]

(32). Ramanathan A; Agarwal PK Evolutionarily Conserved Linkage between Enzyme Fold, Flexibility, and Catalysis. Plos. Biol. 2011, 9, DOI: 10.1371/journal.pbio.1001193.

(33). Norberg AL; Dybvik AI; Zakariassen H; Mormann M; Peter-Katalinić J; Eijsink VGH; Sørlie M Substrate Positioning in Chitinase a, a Processive Chito-Biohydrolase from Serratia Marcescens. FEBS Lett. 2011, 585, 2339–2344, DOI: 10.1016/j.febslet.2011.06.002. [PubMed: 21683074]

(34). Bhowmick A; Sharma SC; Head-Gordon T The Importance of the Scaffold for de Novo Enzymes: A Case Study with Kemp Eliminase. J. Am. Chem. Soc 2017, 139, 5793–5800, DOI: 10.1021/jacs.6b12265. [PubMed: 28383910]

(35). Bhowmick A; Sharma SC; Honma H; Head-Gordon T The Role of Side Chain Entropy and Mutual Information for Improving the de Novo Design of Kemp Eliminases KE07 and KE70. Phys. Chem. Chem. Phys 2016, 18, 19386–19396, DOI: 10.1039/c6cp03622h From NLM Medline. [PubMed: 27374812]

(36). Ruscio JZ; Kohn JE; Ball KA; Head-Gordon T The Influence of Protein Dynamics on the Success of Computational Enzyme Design. J. Am. Chem. Soc 2009, 131, 14111–14115, DOI: 10.1021/ja905396s. [PubMed: 19788332]

(37). Thielges MC; Chung JK; Fayer MD Protein Dynamics in Cytochrome P450 Molecular Recognition and Substrate Specificity Using 2D IR Vibrational Echo Spectroscopy. J. Am. Chem. Soc 2011, 133, 3995–4004, DOI: 10.1021/ja109168h. [PubMed: 21348488]

(38). Liao QH; Kulkarni Y; Sengupta U; Petrovic D; Mulholland AJ; van der Kamp MW; Strodel B; Kamerlin SCL Loop Motion in Triosephosphate Isomerase Is Not a Simple Open and Shut Case. J. Am. Chem. Soc 2018, 140, 15889–15903, DOI: 10.1021/jacs.8b09378. [PubMed: 30362343]

(39). Hong NS; Petrovic D; Lee R; Gryn'ova G; Purg M; Saunders J; Bauer P; Carr PD; Lin CY; Mabbitt PD; et al. The Evolution of Multiple Active Site Configurations in a Designed Enzyme.

Nat. Commun 2018, 9, 3900, DOI: 10.1038/s41467-018-06305-y From NLM Medline. [PubMed: 30254369]

(40). Hamre AG; Jana S; Reppert NK; Payne CM; Sorlie M Processivity, Substrate Positioning, and Binding: The Role of Polar Residues in a Family 18 Glycoside Hydrolase. Biochemistry 2015, 54, 7292–7306, DOI: 10.1021/acs.biochem.5b00830. [PubMed: 26503416]

(41). Patra N; Ioannidis EI; Kulik HJ Computational Investigation of the Interplay of Substrate Positioning and Reactivity in Catechol O-Methyltransferase. Plos One 2016, 11, DOI: 10.1371/journal.pone.0161868.

(42). Hu SS; Offenbacher AR; Thompson EM; Gee CL; Wilcoxen J; Carr CAM; Prigozhin DM; Yang V; Alber T; Britt RD; et al. Biophysical Characterization of a Disabled Double Mutant of Soybean Lipoxygenase: The “Undoing” of Precise Substrate Positioning Relative to Metal Cofactor and an Identified Dynamical Network. J. Am. Chem. Soc 2019, 141, 1555–1567, DOI: 10.1021/jacs.8b10992. [PubMed: 30645119]

(43). Mehmood R; Qi HW; Steeves AH; Kulik HJ The Protein’s Role in Substrate Positioning and Reactivity for Biosynthetic Enzyme Complexes: The Case of SyrB2/SyrB1. ACS Catal. 2019, 9, 4930–4943, DOI: 10.1021/acscatal.9b00865.

(44). Yabukarski F; Biel JT; Pinney MM; Doukov T; Powers AS; Fraser JS; Herschlag D Assessment of Enzyme Active Site Positioning and Tests of Catalytic Mechanisms through X-Ray-Derived Conformational Ensembles. Proc. Natl. Acad. Sci. U. S. A 2020, 117, 33204–33215, DOI: 10.1073/pnas.2011350117 From NLM Medline. [PubMed: 33376217]

(45). Mehmood R; Vennelakanti V; Kulik HJ Spectroscopically Guided Simulations Reveal Distinct Strategies for Positioning Substrates to Achieve Selectivity in Nonheme Fe(II)/Alpha-Ketoglutarate-Dependent Halogenases. ACS Catal. 2021, 11, 12394–12408, DOI: 10.1021/acscatal.1c03169.

(46). Jiang Y; Yan B; Chen Y; Juarez RJ; Yang ZJ Molecular Dynamics-Derived Descriptor Informs the Impact of Mutation on the Catalytic Turnover Number in Lactonase across Substrates. J. Phys. Chem. B 2022, 126, 2486–2495, DOI: 10.1021/acs.jpcb.2c00142 From NLM Medline. [PubMed: 35324218]

(47). Siegel JB; Zanghellini A; Lovick HM; Kiss G; Lambert AR; Clair JLS; Gallaher JL; Hilvert D; Gelb MH; Stoddard BL; et al. Computational Design of an Enzyme Catalyst for a Stereoselective Bimolecular Diels-Alder Reaction. Science 2010, 329, 309–313, DOI: 10.1126/science.1190239. [PubMed: 20647463]

(48). Blomberg R; Kries H; Pinkas DM; Mittl PRE; Grutter MG; Privett HK; Mayo SL; Hilvert D Precision Is Essential for Efficient Catalysis in an Evolved Kemp Eliminase. Nature 2013, 503, 418−+, DOI: 10.1038/nature12623. [PubMed: 24132235]

(49). Broom A; Rakotoharisoa RV; Thompson MC; Zarifi N; Nguyen E; Mukhametzhanov N; Liu L; Fraser JS; Chica RA Ensemble-Based Enzyme Design Can Recapitulate the Effects of Laboratory Directed Evolution in Silico. Nat. Commun 2020, 11, DOI: 10.1038/s41467-020-18619-x.

(50). Khersonsky O; Kiss G; Rothlisberger D; Dym O; Albeck S; Houk KN; Baker D; Tawfik DS Bridging the Gaps in Design Methodologies by Evolutionary Optimization of the Stability and Proficiency of Designed Kemp Eliminase KE59. Proc. Natl. Acad. Sci. U. S. A 2012, 109, 10358–10363, DOI: 10.1073/pnas.1121063109. [PubMed: 22685214]

(51). Haataja T; Gado JE; Nutt A; Anderson NT; Nilsson M; Momeni MH; Isaksson R; Valjamae P; Johansson G; Payne CM; et al. Enzyme Kinetics by GH7 Cellobiohydrolases on Chromogenic Substrates Is Dictated by Non-Productive Binding: Insights from Crystal Structures and MD Simulation. FEBS J. 2023, 290, 379–399, DOI: 10.1111/febs.16602. [PubMed: 35997626]

(52). Offenbacher AR; Sharma A; Doan PE; Klinman JP; Hoffman BM The Soybean Lipoxygenase-Substrate Complex: Correlation between the Properties of Tunneling-Ready States and Endor-Detected Structures of Ground States. Biochemistry 2020, 59, 901–910, DOI: 10.1021/acs.biochem.9b00861. [PubMed: 32022556]

(53). Cameron CE; Benkovic SJ Evidence for a Functional Role of the Dynamics of Glycine-121 of Dihydrofolate Reductase Obtained from Kinetic Analysis of a Site-Directed Mutant. Biochemistry 1997, 36, 15792–15800, DOI: 10.1021/bi9716231. [PubMed: 9398309]

(54). Rajagopalan PTR; Lutz S; Benkovic SJ Coupling Interactions of Distal Residues Enhance Dihydrofolate Reductase Catalysis: Mutational Effects on Hydride Transfer Rates. Biochemistry 2002, 41, 12618–12628, DOI: 10.1021/bi026369d. [PubMed: 12379104]

(55). Wang L; Tharp S; Selzer T; Benkovic SJ; Kohen A Effects of a Distal Mutation on Active Site Chemistry. Biochemistry 2006, 45, 1383–1392, DOI: 10.1021/bi0518242. [PubMed: 16445280]

(56). Roston D; Kohen A; Doron D; Major DT Simulations of Remote Mutants of Dihydrofolate Reductase Reveal the Nature of a Network of Residues Coupled to Hydride Transfer. J. Comput. Chem 2014, 35, 1411–1417, DOI: 10.1002/jcc.23629. [PubMed: 24798860]

(57). Otten R; Padua RAP; Bunzel HA; Nguyen V; Pitsawong W; Patterson M; Sui S; Perry SL; Cohen AE; Hilvert D; et al. How Directed Evolution Reshapes the Energy Landscape in an Enzyme to Boost Catalysis. Science 2020, 370, 1442–1446, DOI: 10.1126/science.abd3623. [PubMed: 33214289]

(58). Hanoian P; Liu CT; Hammes-Schiffer S; Benkovic S Perspectives on Electrostatics and Conformational Motions in Enzyme Catalysis. Acc. Chem. Res 2015, 48, 482–489, DOI: 10.1021/ar500390e. [PubMed: 25565178]

(59). Warshel A Electrostatic Origin of the Catalytic Power of Enzymes and the Role of Preorganized Active Sites. J. Biol. Chem 1998, 273, 27035–27038, DOI: 10.1074/jbc.273.42.27035. [PubMed: 9765214]

(60). Welborn VV; Head-Gordon T Computational Design of Synthetic Enzymes. Chem. Rev 2019, 119, 6613–6630, DOI: 10.1021/acs.chemrev.8b00399. [PubMed: 30277066]

(61). Vaissier V; Sharma SC; Schaettle K; Zhang T; Head-Gordon T Computational Optimization of Electric Fields for Improving Catalysis of a Designed Kemp Eliminase. ACS Catal. 2018, 8, 219–227, DOI: 10.1021/acscatal.7b03151.

(62). Yang ZY; Liu F; Steeves AH; Kulik HJ Quantum Mechanical Description of Electrostatics Provides a Unified Picture of Catalytic Action across Methyltransferases. J. Phys. Chem. Lett 2019, 10, 3779–3787, DOI: 10.1021/acs.jpclett.9b01555. [PubMed: 31244268]

(63). Wu YF; Fried SD; Boxer SG A Preorganized Electric Field Leads to Minimal Geometrical Reorientation in the Catalytic Reaction of Ketosteroid Isomerase. J. Am. Chem. Soc 2020, 142, 9993–9998, DOI: 10.1021/jacs.0c00383. [PubMed: 32378409]

(64). Fried SD; Boxer SG Electric Fields and Enzyme Catalysis. Annu. Rev. Biochem 2017, 86, 387–415, DOI: 10.1146/annurev-biochem-061516-044432. [PubMed: 28375745]

(65). Fried SD; Boxer SG Measuring Electric Fields and Noncovalent Interactions Using the Vibrational Stark Effect. Acc. Chem. Res 2015, 48, 998–1006, DOI: 10.1021/ar500464j. [PubMed: 25799082]

(66). Wolfenden R Transition State Analog Inhibitors and Enzyme Catalysis. Annu. Rev. Biophys. Bioeng 1976, 5, 271–306, DOI: 10.1146/annurev.bb.05.060176.001415. [PubMed: 7991]

(67). Bruice TC; Benkovic SJ Chemical Basis for Enzyme Catalysis. Biochemistry 2000, 39, 6267–6274, DOI: 10.1021/bi0003689. [PubMed: 10828939]

(68). Schramm VL Enzymatic Transition States and Transition State Analogues. Curr. Opin. Struct. Biol 2005, 15, 604–613, DOI: 10.1016/j.sbi.2005.10.017. [PubMed: 16274984]

(69). Simón L; Goodman JM Hydrogen-Bond Stabilization in Oxyanion Holes: Grand Jeté to Three Dimensions. Org. Biomol. Chem 2012, 10, 1905–1913, DOI: 10.1039/c2ob06717j. [PubMed: 22273994]

(70). Burschowsky D; van Eerde A; Ökvist M; Kienhöfer A; Kast P; Hilvert D; Krengel U Electrostatic Transition State Stabilization Rather Than Reactant Destabilization Provides the Chemical Basis for Efficient Chorismate Mutase Catalysis. Proc. Natl. Acad. Sci. U. S. A 2014, 111, 17516–17521, DOI: 10.1073/pnas.1408512111. [PubMed: 25422475]

(71). Warshel A; Sharma PK; Kato M; Xiang Y; Liu HB; Olsson MHM Electrostatic Basis for Enzyme Catalysis. Chem. Rev 2006, 106, 3210–3235, DOI: 10.1021/cr0503106. [PubMed: 16895325]

(72). Lameira J; Bora RP; Chu ZT; Warshel A Methyltransferases Do Not Work by Compression, Cratic, or Desolvation Effects, but by Electrostatic Preorganization. Proteins 2015, 83, 318–330, DOI: 10.1002/prot.24717. [PubMed: 25388538]

(73). Jindal G; Warshel A Misunderstanding the Preorganization Concept Can Lead to Confusions About the Origin of Enzyme Catalysis. Proteins 2017, 85, 2157–2161, DOI: 10.1002/prot.25381. [PubMed: 28905418]

(74). Rothlisberger D; Khersonsky O; Wollacott AM; Jiang L; DeChancie J; Betker J; Gallaher JL; Althoff EA; Zanghellini A; Dym O; et al. Kemp Elimination Catalysts by Computational Enzyme Design. Nature 2008, 453, 190–195, DOI: 10.1038/nature06879. [PubMed: 18354394]

(75). Shao Q; Jiang Y; Yang ZJ EnzyHTP: A High-Throughput Computational Platform for Enzyme Modeling. J. Chem. Inf. Model 2022, 62, 647–655, DOI: 10.1021/acs.jcim.1c01424. [PubMed: 35073075]

(76). Alexandrova AN; Rothlisberger D; Baker D; Jorgensen WL Catalytic Mechanism and Performance of Computationally Designed Enzymes for Kemp Elimination. J. Am. Chem. Soc 2008, 130, 15907–15915, Article, DOI: 10.1021/ja804040s. [PubMed: 18975945]

(77). Khersonsky O; Rothlisberger D; Dym O; Albeck S; Jackson CJ; Baker D; Tawfik DS Evolutionary Optimization of Computationally Designed Enzymes: Kemp Eliminases of the KE07 Series. J. Mol. Biol 2010, 396, 1025–1042, DOI: 10.1016/j.jmb.2009.12.031. [PubMed: 20036254]

(78). Caselle EA; Yoon JH; Bhattacharya S; Rempillo JJL; Lengyel Z; D'Souza A; Moroz YS; Tolbert PL; Volkov AN; Forconi M; et al. Kemp Eliminases of the Alleycat Family Possess High Substrate Promiscuity. ChemCatChem 2019, 11, 1425–1430, DOI: 10.1002/cctc.201801994 From NLM PubMed-not-MEDLINE. [PubMed: 31788134]

(79). Wang PY; Zhang J; Zhang SY; Lu DN; Zhu YS Using High-Throughput Molecular Dynamics Simulation to Enhance the Computational Design of Kemp Elimination Enzymes. J. Chem. Inf. Model 2023, 63, 1323–1337, DOI: 10.1021/acs.jcim.3c00002. [PubMed: 36782360]

(80). Jiang Y; Stull SL; Shao Q; Yang ZJ Convergence in Determining Enzyme Functional Descriptors across Kemp Eliminase Variants. Electron. Struct 2022, 4, DOI: 10.1088/2516-1075/acad51.

(81). Gutierrez-Rus LI; Alcalde M; Risso VA; Sanchez-Ruiz JM Efficient Base-Catalyzed Kemp Elimination in an Engineered Ancestral Enzyme. Int. J. Mol. Sci 2022, 23, DOI: 10.3390/ijms23168934.

(82). Shao Q; Jiang Y; Yang ZJ EnzyHTP Computational Directed Evolution with Adaptive Resource Allocation. J. Chem. Inf. Model 2023, DOI: 10.1021/acs.jcim.3c00618 From NLM Publisher.

(83). Park H; Bradley P; Greisen P; Liu Y; Mulligan VK; Kim DE; Baker D; DiMaio F Simultaneous Optimization of Biomolecular Energy Functions on Features from Small Molecules and Macromolecules. J. Chem. Theory Comput 2016, 12, 6201–6212, DOI: 10.1021/acs.jctc.6b00819. [PubMed: 27766851]

(84). Frenz B; Lewis SM; King I; DiMaio F; Park H; Song YF Prediction of Protein Mutational Free Energy: Benchmark and Sampling Improvements Increase Classification Accuracy. Front. Bioeng. Biotech 2020, 8, DOI: 10.3389/fbioe.2020.558247.

(85). Park C Visual Interpretation of the Meaning of Kcat/Km in Enzyme Kinetics. J. Chem. Educ 2022, DOI: 10.1021/acs.jchemed.1c01268.

(86). Baath JA; Jensen K; Borch K; Westh P; Kari J Sabatier Principle for Rationalizing Enzymatic Hydrolysis of a Synthetic Polyester. JACS Au 2022, 2, 1223–1231, DOI: 10.1021/jacsau.2c00204. [PubMed: 35647598]

(87). Schaller KS; Molina GA; Kari J; Schiano-Di-Cola C; Sorensen TH; Borch K; Peters GHJ; Westh P Virtual Bioprospecting of Interfacial Enzymes: Relating Sequence and Kinetics. ACS Catal. 2022, 12, 7427–7435, DOI: 10.1021/acscatal.2c02305.

(88). Kari J; Schaller K; Molina GA; Borch K; Westh P The Sabatier Principle as a Tool for Discovery and Engineering of Industrial Enzymes. Curr. Opin. Biotechnol 2022, 78, DOI: 10.1016/j.copbio.2022.102843.

(89). Wodrich MD; Sawatlon B; Busch M; Corminboeuf C The Genesis of Molecular Volcano Plots. Acc. Chem. Res 2021, 54, 1107–1117, DOI: 10.1021/acs.accounts.0c00857. [PubMed: 33570407]

(90). Xie WJ; Warshel A Natural Evolution Provides Strong Hints About Laboratory Evolution of Designer Enzymes. Proc. Natl. Acad. Sci. U. S. A 2022, 119, DOI: 10.1073/pnas.2207904119.

(91). Amber 2018; University of California, San Francisco, 2018.

(92). Gaussian 16 Rev. C.01; Wallingford, CT, 2016.

(93). Ufimtsev IS; Martinez TJ Quantum Chemistry on Graphical Processing Units. 3. Analytical Energy Gradients, Geometry Optimization, and First Principles Molecular Dynamics. J. Chem. Theory Comput 2009, 5, 2619–2628, DOI: 10.1021/ct9003004 From NLM PubMed-not-MEDLINE. [PubMed: 26631777]

(94). Titov AV; Ufimtsev IS; Luehr N; Martinez TJ Generating Efficient Quantum Chemistry Codes for Novel Architectures. J. Chem. Theory Comput 2013, 9, 213–221, DOI: 10.1021/ct300321a From NLM PubMed-not-MEDLINE. [PubMed: 26589024]

(95). The Pymol Molecular Graphics System, *Version* 2.4; 2015.

(96). Graphpad Prism Version 8.3.1 for Macos; 2019.

(97). Towns J; Cockerill T; Dahan M; Foster I; Gaither K; Grimshaw A; Hazlewood V; Lathrop S; Lifka D; Peterson GD; et al. XSEDE: Accelerating Scientific Discovery. Comput. Sci. Eng 2014, 16, 62–74, DOI: 10.1109/Mcse.2014.80.

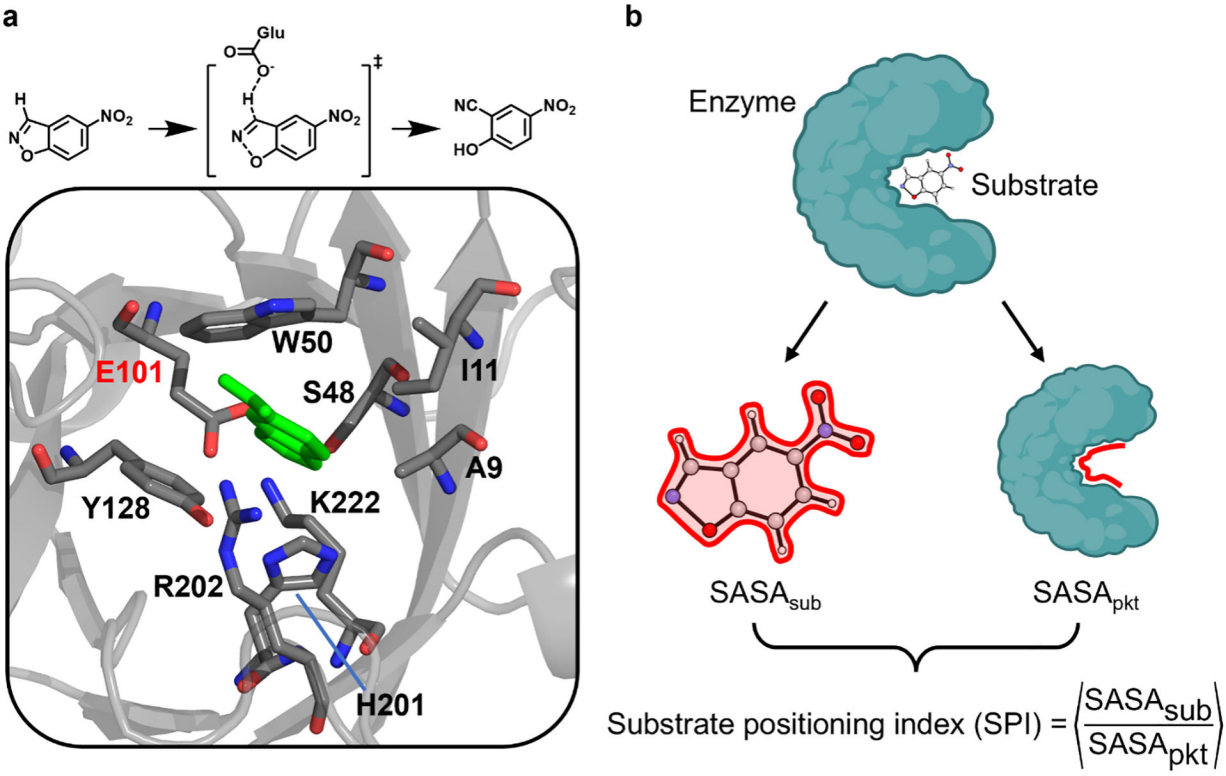

Figure 1.

(a) The model enzyme, Kemp eliminase, used in the study and (b) the schematic definition of substrate positioning index, SPI. (a, *top*) A putative reaction mechanism. The carboxylic group of Glu101 deprotonates the C–H bond on the substrate, 5-nitro-1,2-benzoxazole. (a, *bottom*) The active site structure of Kemp eliminase, KE07-R7–2. The active site residues and the substrate are shown in stick. The substrate is shown in green, and the carbon, oxygen, and nitrogen of the residues are shown in gray, red, and blue, respectively. The catalytic base is labeled in red, and others are labeled in black. The structure is derived from the crystal structure with a PDB ID of 5D38.[39] (b) The solvent-accessible surface area (SASA) of the substrate ($SASA_{sub}$) and enzyme pocket ($SASA_{pkt}$) are evaluated separately by isolating these two parts from the complex. The SPI value is computed as an average over all snapshots sampled along the MD trajectories.

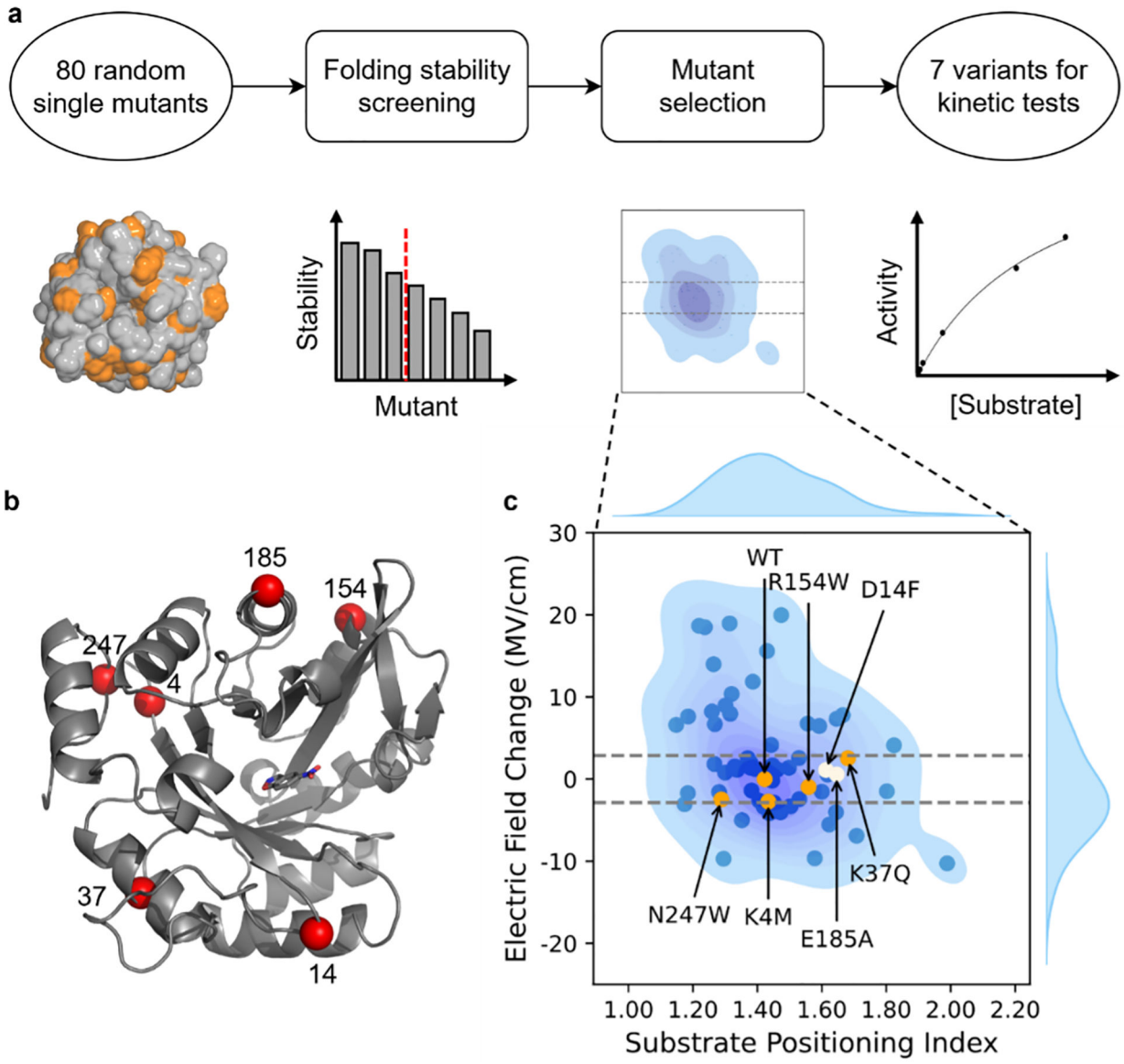

Figure 2.

The computational protocol for the selection of KE variants for kinetic assessment. (a) Computational workflow to screen for mutants with a single amino acid substitution that significantly affects the substrate positioning dynamics but minimally the electric field strength on the breaking bond. (b) The structure of KE07 with the C_α atoms of mutation sites highlighted as red spheres. The structure is the KE07 design model by Röthlisberger *et al.*[74] (c) Distribution of the electric field change, ΔEF_{C-H} versus the substrate positioning index, SPI. The ΔEF_{C-H} of WT is set to be the reference (0 MV/cm). The dashed lines show the EF_{C-H} range cutoff from which mutants with a small electrostatic effect were selected. The dots include the data points for 63 KE variants, including 61 randomly generated variants that pass the folding stability test, E185A reported by Bhowmick *et al.*[35], and the wild-type KE07-R7–2 enzyme. Orange and white dots are the mutants selected for the first and second rounds of kinetic characterization, respectively. Other mutants are shown in blue.

The blue shade under the dots shows the data distribution in the 2D space and the curves with blue fill on the sides show the data distribution of EF_{C-H} or SPI. The shade and curves are derived from fitting all 63 data points using Kernel Density Estimation (Text S1).

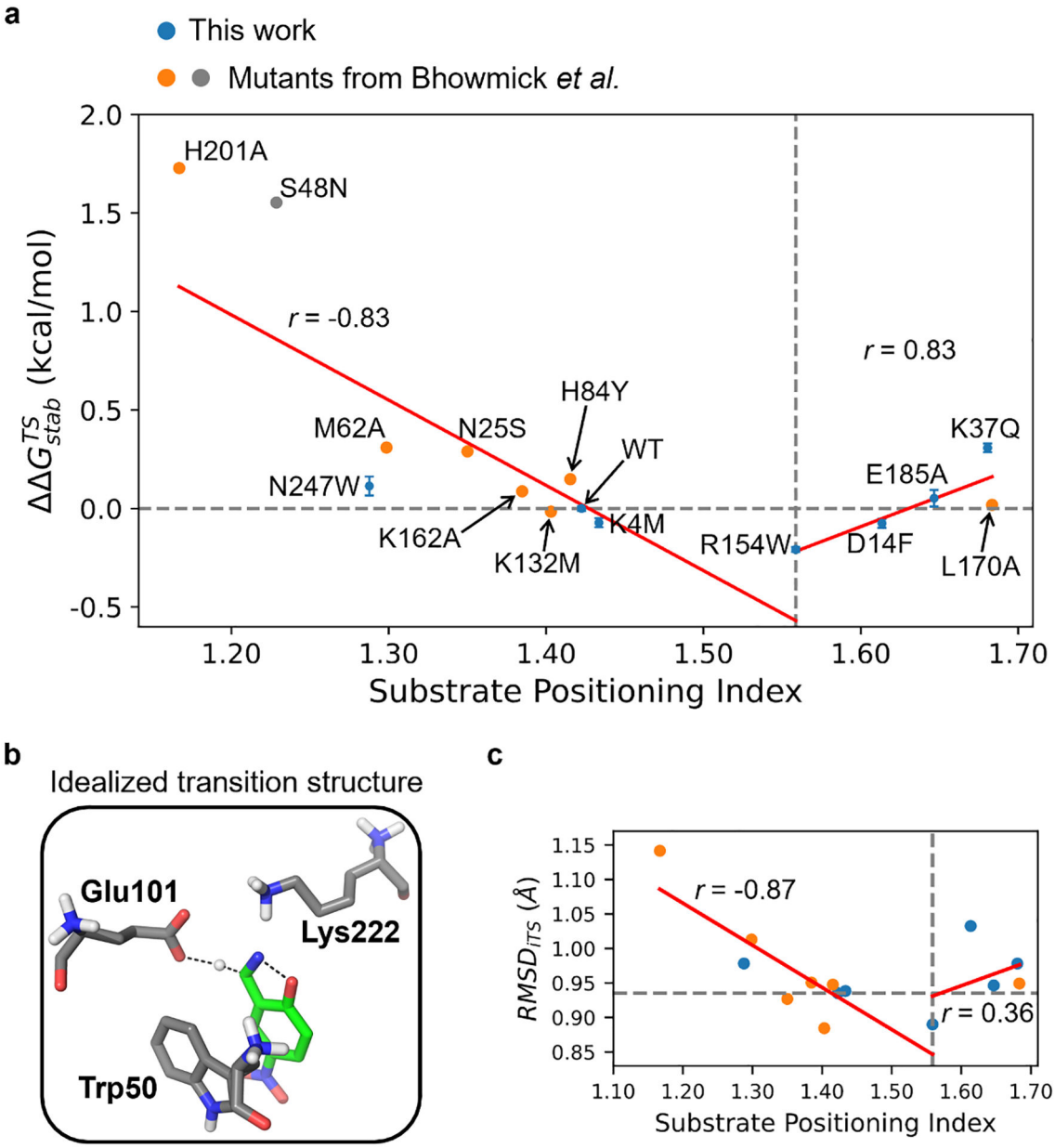

Figure 3.

The impact of substrate positioning dynamics on the activation barrier and reaction conformation for KE07-R7–2 variants that are experimentally tested in this work (blue) and reported by Bhowmick *et al.*[35] (orange and gray). (a) The correlation between change of activation free energy $(\Delta\Delta G^{TS}_{stab})$ versus the substrate positioning index (SPI). For each data point tested in this work, the mean and standard error (shown as the vertical error bar) are derived from three independently repeated kinetic measurements. The horizontal dashed line indicates the position of $\Delta\Delta G^{TS}_{stab} = 0$. The vertical dashed line indicates the position of SPI = 1.56 where the beneficial mutant R154W is located. The vertical dashed line is also the boundary of the two-segment piecewise linear fitting. The fitting lines are shown in red and labeled with the corresponding Pearson correlation coefficient (r). The data point of R154W

is included in both fitting lines. S48N is not included in the fitting because its electric field strength is outside the selection window of ±2.88 MV/cm. (b) Structure of the idealized transition state optimized from QM calculations.[74] The dashed lines indicate the breaking or forming bonds. (c) Scatter plots for the root-mean-square deviation from the idealized transition state, i.e., $RMSD_{iTS}$ versus SPI of the selected KE07-R7–2 variants. The dashed and red lines are drawn similarly to (a). The horizontal dashed line indicates the value of WT $RMSD_{iTS}$ (0.94 Å).

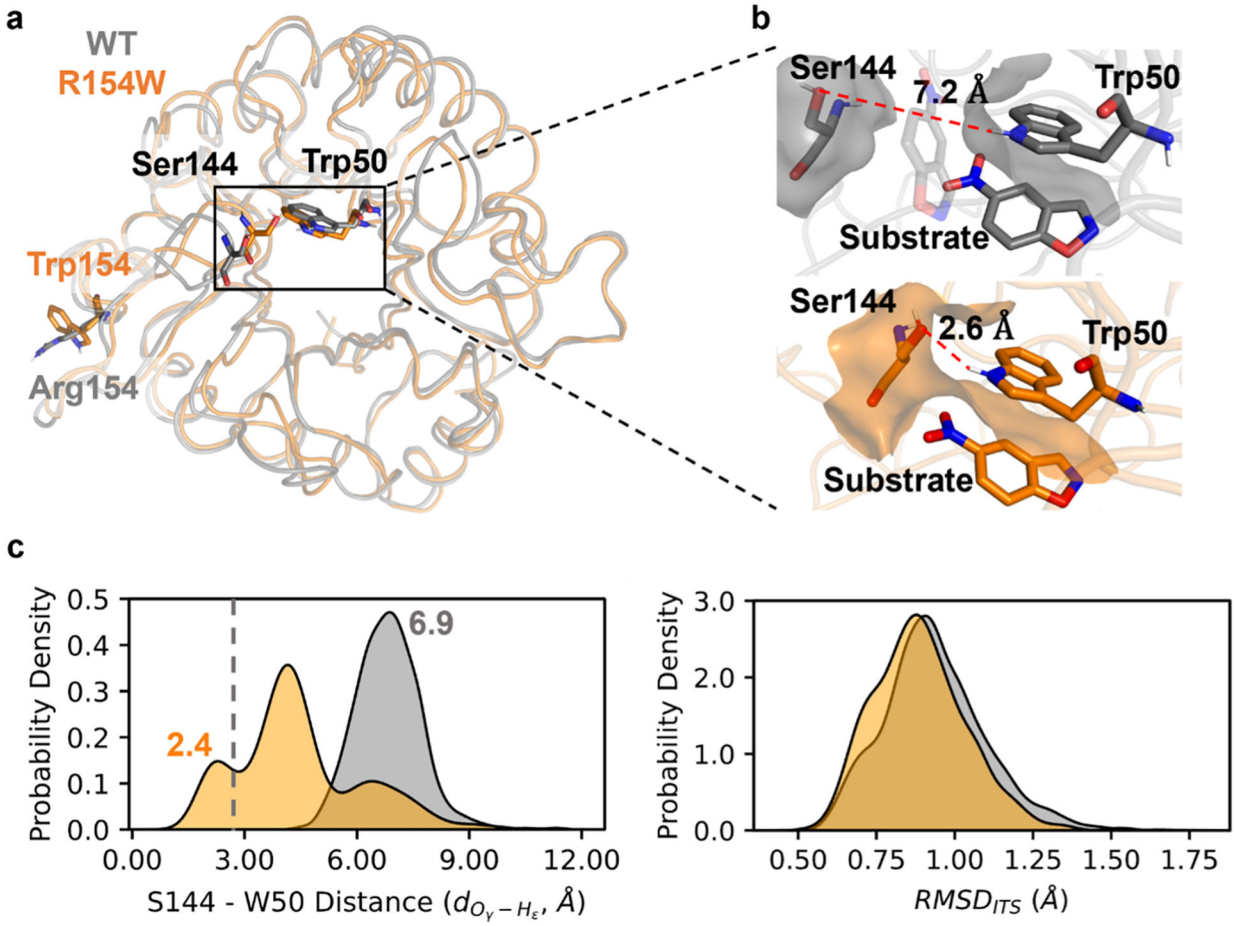

Figure 4.

The molecular mechanism underlying the impact of R154W mutation on substrate positioning dynamics. (a) Structure overlay of the representative conformation of WT (gray) and R154W (orange) with the residues at the sites of 50, 144, and 154 shown in stick. The structures of the representative conformation are chosen from MD trajectories based on the S144 – W50 distance $(d_{O_\gamma - H_\varepsilon})$, that is, picked randomly from structures that have the distance in the range of 6.9 ± 0.3 and 2.4 ± 0.3 Å for WT and R154W, respectively. They are peak values of the distance distribution shown in Figure 4c *left*. (b) Surfaces of Trp50 and Ser144 in WT and R154W. The distance between Ser144 O_γ and Trp50 H_ε, $d_{O_\gamma - H_\varepsilon}$, is shown as the red dashed line. The opaque substrate indicates its favorable position in the active site, while the transparent substrate illustrates a potentially unfavorable position in the WT. This unfavorable position is a conceptual illustration since it is prohibited by the constraints applied during the MD simulation. (c) Distribution of the distance between Ser144 O_γ and Trp50 H_ε, $d_{O_\gamma - H_\varepsilon}$ in the WT and R154W (*left*) and RMSD to the idealized transition station (*right*). In the $d_{O_\gamma - H_\varepsilon}$ distribution, the gray vertical dashed line represents the sum of van der Waals radii for oxygen and hydrogen (2.72 Å). The curves are made by fitting the corresponding data from all snapshots from MD using Kernel Density Estimation (Text S1).

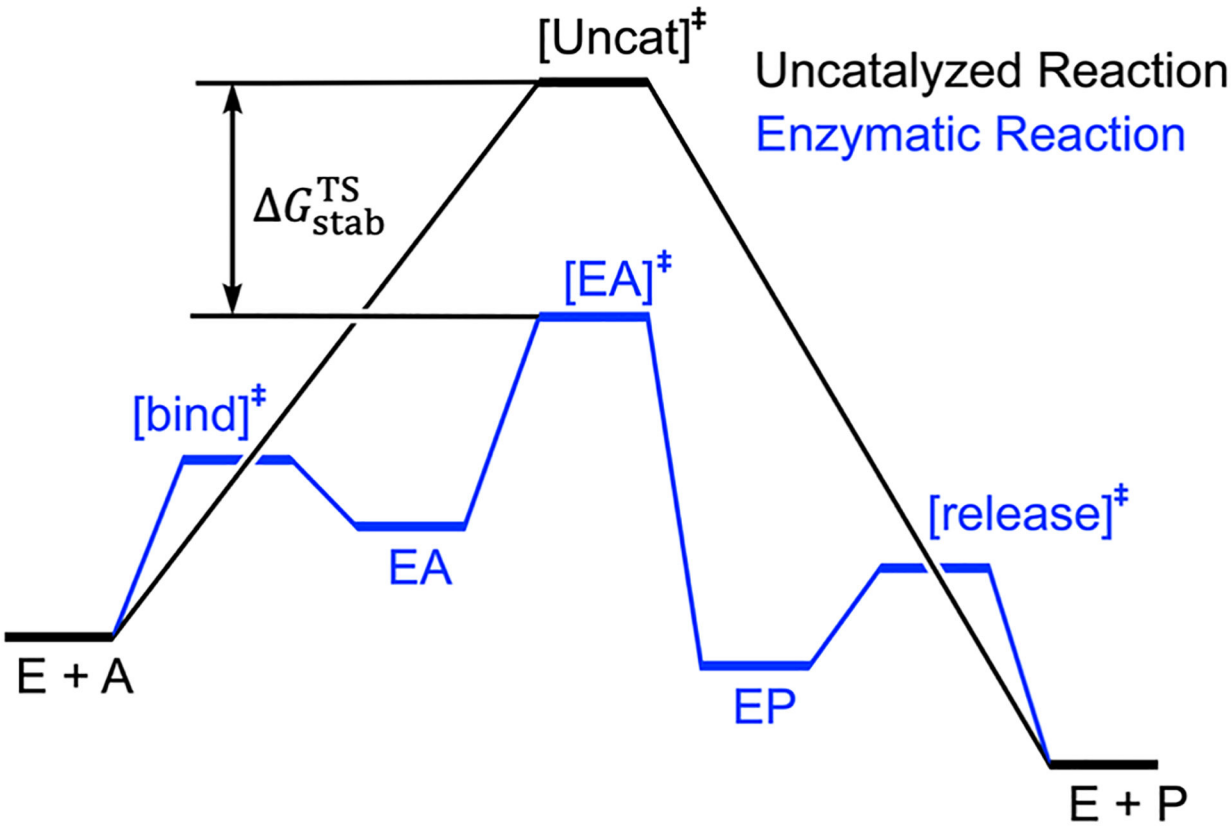

Scheme 1.

The definition of ΔG_{stab}^{TS} through a conceptual energy profile of enzymatic reaction (in blue) and uncatalyzed reaction (in black). [EA]‡ and [Uncat]‡ are transition states for the enzymatic reaction and uncatalyzed reaction, respectively. E, A, EA, EP, P are enzyme, substrate, enzyme-substrate complex, enzyme-product complex, and product, respectively. [bind]‡ and [release]‡ are transition states for the substrate binding and product release, respectively. ΔG_{stab}^{TS} is the transition state (TS) stabilization free energy.